Advances in Mechanical and Materials Engineering

Volume 40, 2023, Pages 203-214
https://doi.org/10.7862/rm.2023.20

THE FACULTY OF MECHANICAL ENGINEERING AND AERONAUTICS
RZESZOW UNIVERSITY OF TECHNOLOGY

Original Research

Design of Newly Developed Burner Rig Operating with Hydrogen Rich Fuel Dedicated for Materials Testing

Wojciech J. Nowak [1,*], Marcin Drajewicz [1], Marek Góral [1], Robert Smusz [2], Piotr Cichosz [3], Andrzej Majka [4], Jarosław Sęp [5]

[1] Department of Materials Science, Faculty of Mechanical Engineering and Aeronautics, Rzeszow University of Technology, Al. Powstanców Warszawy 12, 35-959 Rzeszów, Poland; drajewic@prz.edu.pl (M. Drajewicz), mgoral@prz.edu.pl (M. Góral)
[2] Thermodynamics Department, Rzeszow University of Technology, Al. Powstańców Warszawy 12, 35-959 Rzeszow, Poland; robsmusz@prz.edu.pl
[3] PROXIMO AERO SP. Z O.O., ul. Dębicka 221 A, 35-213 Rzeszów, Poland; piotr.cichosz@proximo.aero
[4] Department of Aircrafts and Aircraft Engines, Rzeszow University of Technology, Al. Powstańców Warszawy 12, 35-959 Rzeszów, Poland; andrzej.majka@prz.edu.pl
[5] Faculty of Mechanical Engineering and Aeronautics, Rzeszow University of Technology, Al. Powstańców Warszawy 12, 35-959 Rzeszów, Poland; jsztmiop@prz.edu.pl

* Correspondence: wjnowak@prz.edu.pl

Received: 15 September 2023 / Accepted: 9 October 2023 / Published online: 13 October 2023

Abstract

The main purpose of present article is to present the burner rig station newly developed at the Rzeszow University of Technology in Poland. The burner rig is dedicated to operate on fuels rich in hydrogen. The burner rig is able to operate with fuels with hydrogen content up to 50 volume %. A detailed description of burner rig construction is presented. Moreover a mathematical model predicting temperature distribution within the combustion chamber is presented. The obtained results showed a good insulation of burner rig construction leading to the temperature gradient from 1674°C in the burner rig to 214°C on steel housing.

Keywords: hydrogen-rich fuel, burner rig, high temperature oxidation, water vapour, high temperature materials

1. Introduction

Alloys used in aircraft engines or in stationary gas turbines (SGT) face harsh conditions, such as high temperature, aggressive gases and cyclic thermal loading. Thus, they need to possess good combinations of mechanical strength, microstructural stability and oxidation resistance. Ni-based alloys are the most common materials used in the hottest part of the gas turbines nowadays. However, the constant need of increase in gas turbines efficiency demands increasing of inlet gases temperature (Schütze & Quadakkers, 2017). Also a strong need of limitation of pollutions from jet engines exhaust exists. This can be achieved by using a hydrogen rich fuel despite gasoline. Combustion of hydrogen rich fuel results in an increase in exhaust gases temperature and higher water vapor content in the exhaust gases. Therefore, the materials used in the gas turbines face not only the higher temperature but also water vapor. It is known from the literature, that water vapor presence in the atmosphere significantly alters oxidation kinetics of the alloys. It was found for pure chromium, that the water vapor presence causes increase of oxidation kinetics accompanied with better chromia scale adherence and formation of blade-shaped oxide (Quadakkers et al., 1996; Michalik et al., 2005; Hänsel et al., 1998; 2003). Differences in oxidation kinetics and the oxide scale morphology formed on Ni-Cr binary alloy during exposure in dry and wet oxygen was found by Essuman et al. (2008) and Żurek et al. (2008), namely oxidation rate was found to be higher in wet atmosphere as compared to dry one. Similar observation on Ni-base alloys during oxidation in dry and humid atmosphere was found by e.g. England and Virkar (1999, 2001). The authors found the oxidation rates in wet hydrogen to be higher by a fac-

tor varying between 8 and 30 compared to air, while at 1100°C the effect of water vapour decreased and the growth rate in wet hydrogen was higher than in dry air by a factor of 1.5 to 13.

One of the effect of water vapor is enhanced chromium evaporation from the surfaces of chromia forming alloys at high temperatures. This phenomenon was extensively investigated e.g. by Opila et al. (2007) and Stanislowski et al. (2007) in high pO_2-gas, e.g. wet air. Chromium oxide can evaporate according to the following reactions:

$$\frac{1}{2}Cr_2O_{3(s)} + \frac{3}{4}O_2 \rightarrow CrO_{3(g)} \tag{1}$$

$$\frac{1}{2}Cr_2O_{3(s)} + H_2O_{(g)} + \frac{3}{4}O_{2(g)} \rightarrow CrO_2(OH)_{2(g)} \tag{2}$$

$$\frac{1}{2}Cr_2O_{3(s)} + \frac{1}{2}H_2O_{(g)} + \frac{1}{2}O_{2(g)} \rightarrow CrO_2(OH)_{(g)} \tag{3}$$

Volatilization of chromium species during high temperature exposure of Ni-base alloys was investigated by many researchers, like e.g. Deodeshmukh (2013a, 2013b), Holcomb (2008) or Pujilaksono et al. (2008). The authors found mass loss of the exposed specimen without oxide scale spallation (Deodeshmukh, 2013b) and formation of blade-shaped oxides (Pujilaksono et al., 2008). It was also claimed, that not only temperature, but also amount of water vapor in the atmosphere has detrimental effect on the rate of volatilization of chromium species (Holcomb, 2008). It was also found by Nowak et al. (2016) that the water vapour suppresses nitrides formation below the external chromia scale on Ni-base superalloy Rene 80. The authors correlated the latter with preferential adsorption of water vapor molecules on the surface and suppressing the nitrogen transport through the oxide scale.

In case of an alumina forming alloys it was found by Maris-Sida et al. (2003) that presence of water vapor in the test atmosphere, strongly enhance spallation of the oxide scale. Onal et al. (2004) found that for alumina forming alloys water vapour adversely affects the selective oxidation of aluminium. The authors concluded that suppression of external oxidation of aluminium may be the result of a more rapid growth of the transient oxides caused by the presence of water vapour. Enhanced spallation of an alumina scale was observed as well. Janakiraman et al. (1999) found that 2 to 4 times increase in weight loss in the presence of water vapor in the atmosphere during cyclic oxidation of Ni-base superalloys. Smialek et al. (2010) found so called desktop spallation (DTS) and moisture-induced delayed spallation (MIDS). In both proposed mechanisms moisture has been postulated to serve as a source of interfacial hydrogen embrittlement. Hydrogen, in this particular case, is derived from reaction with aluminium in the alloy at an exposed interface.

Considering all findings mentioned above there is a strong need to find a materials exhibiting better performance at elevated temperature and increased water vapor content. Such materials can be e.g. high entropy alloys (e.g. NiCoCrAlFe) or materials covered by protective coatings, like e.g. thermal barrier coatings (TBC) or environmental barrier coatings (EBC). Typically for conventional fuel gas turbines the thermal barrier coatings are used for protection of Nickel-superalloys surface material (Grilli et al., 2021; Suzuki et al., 2022). The outer ceramic layer contains usually yttria stabilized zirconia oxide (YSZ) (Golewski and Sadowski, 2019) or pyrochlores (Pędrak et al., 2021; 2022). The bond coat protects surface against oxidation and hot corrosion and might be formed from MCrAlY-type alloys (Zakeri et al., 2022) or by production of aluminide coatings (Góral et al., 2021; Kopec et al., 2021). For production of TBCs different method might be uses such as diffusion aluminizing (Cocojaru et al., 2022), atmospheric plasma spraying (Girolamo et al., 2014) or electron beam physical vapour deposition (EB—PVD) (Qiu et al., 2021). In new Environmental Barrier Coatings (EBC) the outer ceramic layer might contain different ceramic materials such as Y_2SiO_5-YS, $Yb_2Si_2O_7$-YDS, $Gd_2Zr_2O_7$, $Y_3Al_5O_{12}$, $Yb_2Si_2O_7$-YDS, Y_2O_3 produced using different thermal spraying processes (Vassen et al., 2019). In the case of hydrogen application as a fuel the water vapor formed during hydrogen burning is formed during reactions (Wang et al., 2020):

$$Yb_2SiO_5(s) + 3H_2O(g) \rightarrow Yb_2Si_2O_7(s) + 2Yb(OH)_3(g), \tag{4}$$

$$Yb_2Si_2O_7(s) + 2H_2O(g) \rightarrow Yb_2SiO_5(s) + Si(OH)_4(g). \quad (5)$$

The silicon is usually used for protection against water vapour in this application (Chen et al., 2021).

However, most of aforementioned materials were examined using mixture of air and water vapor. Investigations of these materials in direct exhaust coming from burning of hydrogen rich fuel is very limited. Thus in the present work a burner rig operating with mixture of fuel and hydrogen is introduced. In this equipment a testing of various materials inside the burner rig is possible, which gives the unique opportunity of testing in real exhaust originating from burning a hydrogen fuel in real operating conditions. Such equipment is installed at the Rzeszow University of Technology (Poland, Subcarpathian region).

The hydrogen is considered as an alternative fuel for Industrial Gas Turbines. Leading IGT manufacturers such as MHI (*Decarbonization technology*, 2023), Siemens (*Zero emission hydrogen turbine center*, 2023), General Electric (*Hydrogen fueled gas turbines*, 2023) are planning the using of fully hydrogen powered gas turbines. The first industrial scale experimental gas turbine fueled by mixture of natural gas and up to 20 % of hydrogen was successfully validated in Plant McDonough-Atkinson facility (USA) on MHI gas turbine (*Southern Co.*, 2023). In Norway the first micro turbine powered by 100% hydrogen fuel was demonstrated in 2022 by Banihabib and Assadi (2022). The small hydrogen power generator based on small gas turbine was developed by Turbotec Company (*Hydrogen gas turbine*, 2023). This type of gas turbines might be connected with renewable energy power plants (wind turbines, photovoltaics (PV)) and used as energy storage unit (Grilli et al., 2021; Pyo et al., 2021). From many years the design and manufacturing research are conducted in the case of gas turbine design (Najjar, 1990; Marin et al., 2021) and materials (Stefan et al., 2022).

The hydrogen might be also used in aeroengines. The B-57 was the first plane, which was tested in 50s for using of hydrogen as a fuel in Curtiss Wright J-65 jet engine. In this solution two independent fuel systems were used, namely one using kerosene and another using hydrogen (Winter, 1990). The using of hydrogen was considered for application of high-speed reconnaissance plane Lockheed CL-400 (Rich, 1973). The Tupolev (Soviet Union) converted the civil Tu-154 for using of hydrogen (Tupolev, 1994). Since 1991 the design of airplane using hydrogen fuel was considered in international cooperation (Westenberger, 2002). Finally the CRYOPLANE European project was run in 2000 (Westenberger, 2003). The other solutions for using of hydrogen for aeroengine applications is using for petrol-powered engines (Boeing, 2010) as well as for fuel-cells proposed (Renouard-Vallet et al., 2011). The application of fuel cells is planned by leading aircraft manufacturers such as Airbus (Airbus, 2023). Hydrogen is a promising fuel for hypersonic planes and was tested on X-43 experimental plane (Moses et al., 2004).

Hydrogen from decades are used for rocket propulsion applications. In the United States the M-1 was the first hydrogen-powered rocket engine (Report 2555-M-1-F, 1967). The J-2 engine was successfully used in Saturn family of rocked used in Apollo program (NASA, 1968). The next generation of cryogenic hydrogen-oxygen (LH/LOX) powered rocket engines R-2S was applied in Space Shuttle as a unit with highest trust in the history (Wilhelm, 1972). Currently the Blue Origin developing the cryogenic BE-3 engine (Cowing, 2012). The similar development of LH/LOX rocket engines took splace in Russia which designed the RD-0120 engine as an equivalent for R-23S engine (Rachuk et al., 1996). This types of engines were also developed in other countries: Japan (Negoro et al., 2007),China (Tan, 2013) and applied in EU - Ariane 5 (Chopinet et al., 2011), and India in GSLV-family rockets (Lele, 2014).

2. Materials and methods

Construction of burner rig dedicated for operation with fuels rich in hydrogen, which is able to operate with fuels with hydrogen content up to 50 volume % was described in details. A schematic pictures showing dimensions and cross-sections of burner rig was presented and explained. Moreover a mathematical model predicting temperature distribution within the combustion chamber is presented. The modelling is done according to algorithm shown in ASTM C 680-08 (2010).

3. Results

3.1. Burner rig description

For a purpose of research activities, new test bench has been designed, a functional research stand for combustion of hydrogen-based mixtures. Combustion chamber allows research of the impact of hydrogen flames on the structure of base materials structure and coatings. The thermodynamical and mechanical design was performed to maximize technical capabilities of the rig, which is able to be feed of a mixture of hydrogen with an oxidant, i.e. air and/or oxygen in the desired proportions up to 50% H_2. Fuel and oxidants are supply to the burner through independent installations controlling pressure, temperature and flow for each medium. An overview of the burner rig is shown in Figure 1.

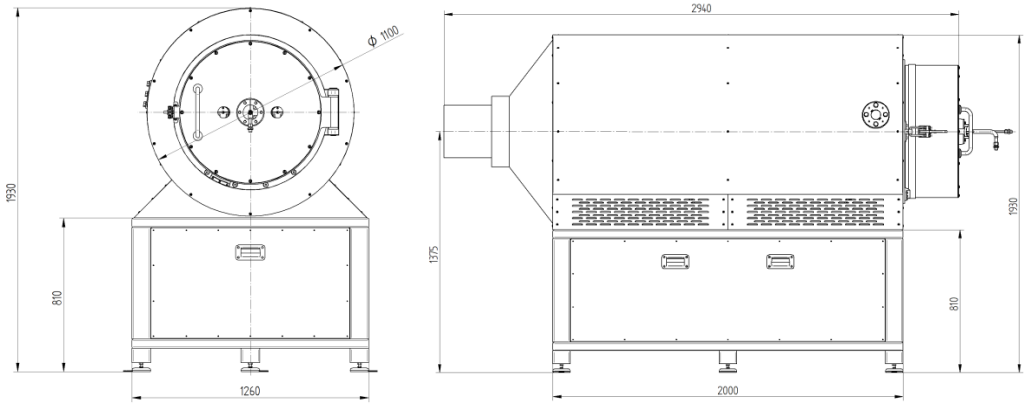

Fig. 1. Front view (a) and side view (b) of burner rig.

The combustion chamber is a cylinder with a base diameter of about 0.15 m and a length of about 0.5 m with a burner and a multi-position mounting bracket for the tests item. It is equipped with an inspection window that allows the observation of the combustion process using cameras as well as temperature measurement for the non-contact method. The chamber enabling simple and quick assembly of the test pieces in the holder and placing it together with the holder in the chamber. In addition to thermal resistance, the chamber must also ensure mechanical strength, as well as must be thermally insulated and protected against accidental contact with hot elements by technical personnel. The combustion chamber is made of refractory concrete (1) (Runcast BWM1), next thermal shock absorbing and sealing compound (Promix ZOR), high temperature insulation (Promaform 1430), medium temperature insulation (Promaform 1260) (4) and steel casing. Inspection window (5) and thermocouple port (6) (Figure 2).

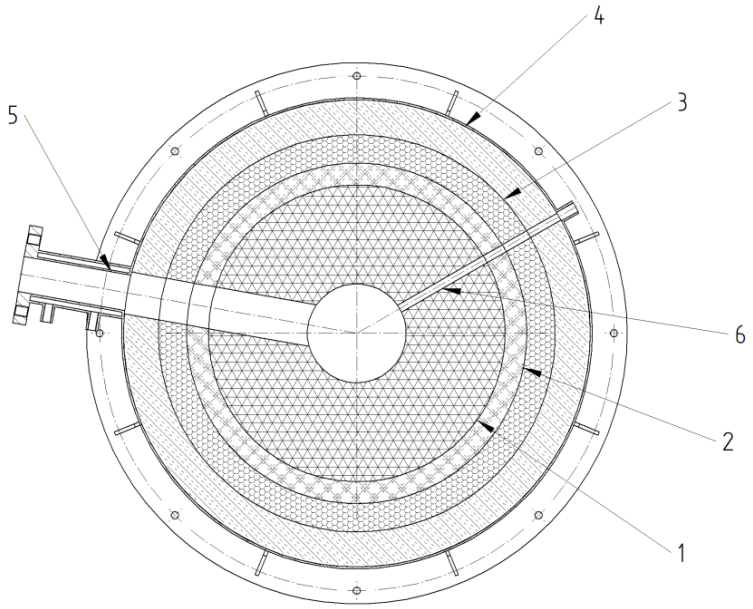

Fig. 2. Cross-section of combustion chamber: 1 – refractory concrete, 2 –insulating concrete layer 1, 3 –insulating concrete layer 2, 4 – medium temperature insulation, 5 – inspection window, 6 – thermocouple port.

The thicknesses and order of the layers have been determined in such a way as to reduce heat loss as much as possible on the one hand, and to minimize thermal stresses that may cause damage to the concrete on the other hand. Burner rig is built up from several segments, including burner, combustion chamber, adiabatic, transition, flue gases cooling and exhaust outlet (Figure 3) and can easily be expanded by adding additional segments in the future depending on demands.

The burner system placed in the chamber have an ignition system and a flame detection system cooperating with the leak control system and automatic fuel cut-off. Flue gas outlet led outside the room to the chimney with measurement of flue gas parameters. The outlet is thermally insulated and ensure tightness. The control system of the stand has been designed and made in a way that allows the preparation of an appropriate mixture for combustion, its control (composition, temperature, flow, pressure, etc.), safe combustion, control of the temperature of the test item and parameters in the combustion chamber itself. The key parameters of the test are register by the data acquisition system (DAQ) and enable data export. The process control is based on the software run on industrial PLC controller. In the future additional capabilities will be incorporated into research rig, therefore some possibility of expanding its functionality in the future has been secured. The control system ensures the ability to remotely conduct the full test cycle and the key element of the control system is an independent safety system guarantees the safety of its operators. The rig is control by HMI (Human Machine Interface), which allows the staff to determine the process parameters and visualize the process itself as well as all measured parameters. Additionally process parameters and measured data can be broadcast using a communication protocol.

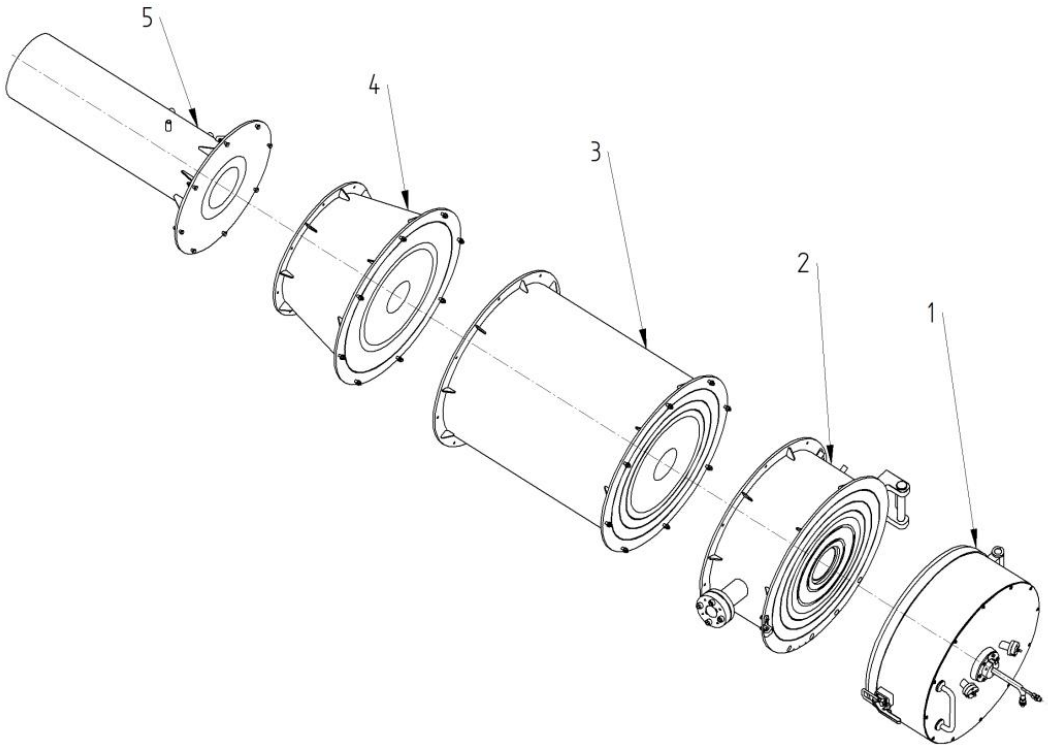

Fig. 3. Modules of combustion chamber: burner (1), combustion chamber (2), adiabatic (3), transition (4), flue gases cooling and exhaust outlet (5).

Research stand is equipped with pressure reducers on each of the connected media along with leakage detection and has the measurement stubs allowing additional measurement of process parameters not resulting from the requirements of the control system and the process safety system.

Main process parameters:

- Burner: 7.5 kW,
- H_2 level: up to 50%,
- Max temp in combustion chamber: 1750°C,
- Max fuel flow: 1.54 m^3/h,
- Max oxidant flow: 11.8 m^3/h,
- Temperature measurement points: 3,
- Total weight: 1300 kg.

Figure 4 depicts the existing burner rig placed in the Hydrogen Laboratory within the Research and Development Laboratory for Aerospace Materials structure. The device is currently being tested.

(a)

(b)

Fig. 4. Images showing the existing burner rig (a) and the control panels (b).

3.2. Modelling of temperature distribution

Based on the mathematical model and algorithm presented in the standard ASTM C 680-08 (2010) the temperature distribution for all layers was calculated. The calculations take into account the variable value of the thermal conductivity coefficient. Perfect contact between materials was established. The heat flux conditions for internal and external surfaces were given by Newton's law of convection.

For the internal side:

$$-k(T)\frac{\partial T}{\partial n} = h_{si}(T_i - T_{si}) \tag{6}$$

where: h_{si} – heat transfer coefficient on the internal boundary, T_i – fluid temperature at the inside boundary, T_{si}—surface temperature on the internal boundary, $k(T)$ – thermal conductivity.

$$-k(T)\frac{\partial T}{\partial n} = h_{se}(T_{se} - T_e) \tag{7}$$

where: h_{se} – heat transfer coefficient, T_e – fluid temperature at the outside boundary, T_{se} – surface temperature on the external boundary of the model. Radiative heat exchange was taken into account on the outer surface.

$$h_{se} = h_{ce} + h_{re} \tag{8}$$

where: h_{re} – component of the heat transfer coefficient due to radiation, h_{ce} – component of the heat transfer coefficient due to convection.

$$h_{re} = \frac{\sigma\varepsilon(T_{se}^4 - T_o^4)}{T_{se} - T_o} \tag{9}$$

where: $\sigma = 5.67 \cdot 10^{-8}$ W/(m^{2}K^4) is the Stefan-Boltzmann constant, ε – is the emissivity of the surface, T_o – surrounding temperature.

To determine the heat transfer coefficient on the internal boundary, the Gnielinski correlation was used, taking into account the influence of the thermophysical properties of the fluid and the thermal entrance region (Gnielinski, 1976):

$$Nu = \frac{\left(\frac{f_D}{8}\right) \cdot (Re - 1000) \cdot Pr}{1 + 12.7 \cdot \left(\frac{f_D}{8}\right)^{0.5} \cdot \left(Pr^{\frac{2}{3}} - 1\right)} \cdot \left[1 + \left(\frac{D_h}{L}\right)^{\frac{2}{3}}\right] \cdot \left(\frac{\eta}{\eta_{wall}}\right)^m \tag{10}$$

where: f_D – Darcy friction factor, D_h –hydraulic diameter of the combustion chamber, L – length of the combustion chamber, Pr – Prandtl number, η – dynamic viscosity of the fluid, Re – Reynolds number, Nu – Nusselt number.

$$m = 0.11 \; if \; \frac{\eta}{\eta_{wall}} < 1 \tag{11}$$

$$m = 0.25 \; if \; \frac{\eta}{\eta_{wall}} > 1 \tag{12}$$

On the other hand, to determine the component of the heat transfer coefficient due to convection on the external boundary, the Churchill and Chu correlation was used (Churchill and Chu, 1975):

$$Nu = \left\{0.6 + \frac{0.387Ra^{1/6}}{\left[1 + \left(\frac{0.559}{Pr}\right)^{9/16}\right]^{8/27}}\right\}^2 \tag{13}$$

where: Ra – Rayleigh number.

The calculated temperature distribution in the combustion chamber is shown in the Figure 5 and Table 1.

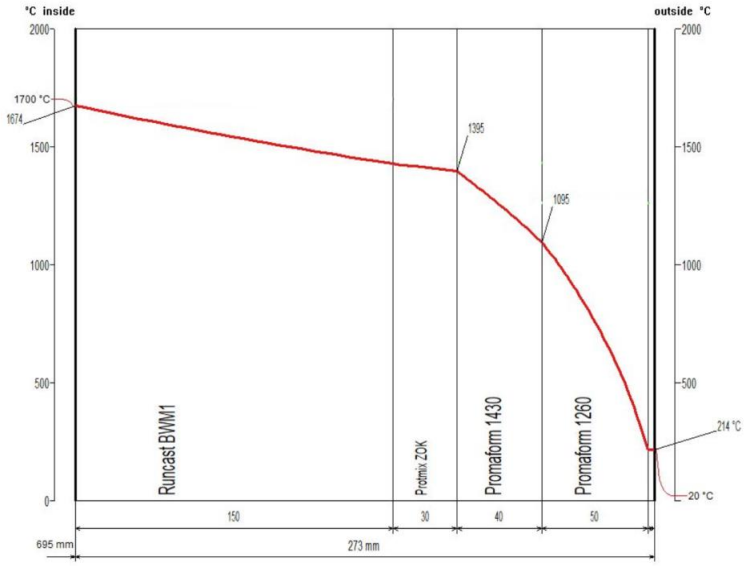

Fig. 5. Calculated temperature distribution in combustion chamber.

Table 1. Layer mean and surface temperature in combustion chamber (NASA, 1968).

Material	Thickness, mm	Surface temp., ℃	Layer mean temp., ℃
Runcast BWM1	150	1674	1536
Protmix ZOR	30	1426	1410
Promaform 1430	40	1395	1249
Promaform 1260	50	1096	720
Steel	3	214.5	214

As can be seen from the Figure 5 high temperature resistant alumina based refractories have low thermal conductivity values (Table 2) which result in deep penetration of temperature into the furnace wall. This requires thick walls of refractory materials to reduce the temperature to an acceptable value for strictly insulating materials. This is a significant limitation that makes it impossible to minimize the dimensions and weight of the furnace. This results in a high heat capacity of the kiln, and thus a large time constant during kiln start-up (Figure 6).

Table 2. Materials thermal properties of furnace (NASA, 1968).

Material	Density, kg/m^3	Layer mean temp., ℃	Mean thermal conductivity, W/m℃
Runcast BWM1	2600	1536	1.98
Protmix ZOR	170	1410	2.6
Promaform 1430	270	1249	0.34
Promaform 1260	390	720	0.14
Steel	7850	214	49

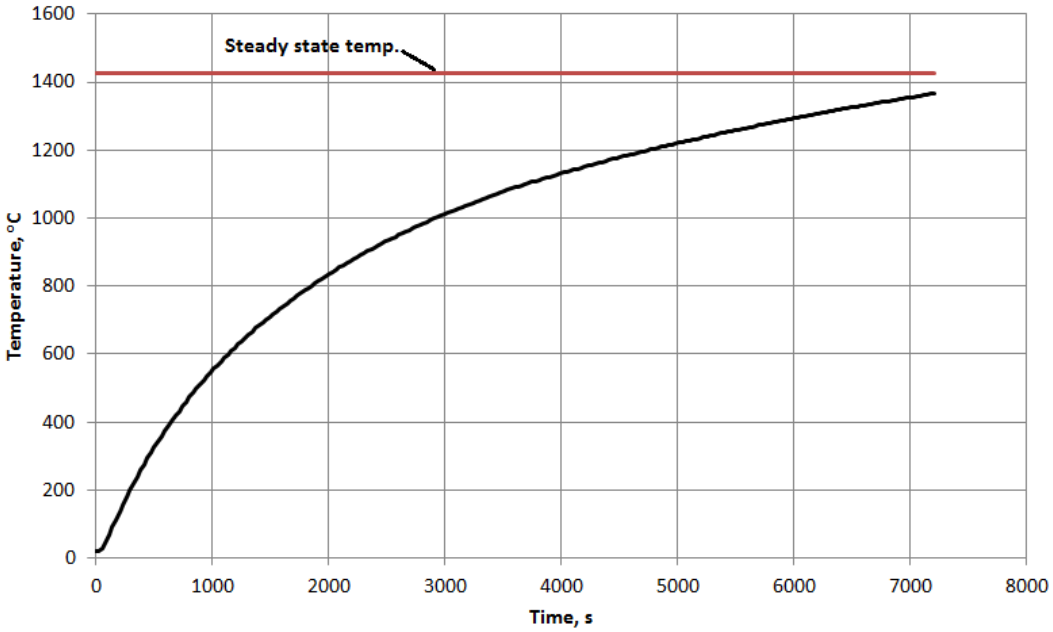

Fig. 6. Temperature at the boundary of Runcast BWM1 and Protmix ZOR layers.

4. Conclusions

Burning of hydrogen enriched fuel leads to increase in operating temperature (comparing to "traditional fuels") as well as in increase in water vapor content in the exhaust gases. The description of burner rig allowed to make a following conclusions:

- The design of used burner allows for using a mixture of traditional fuels (e.g. methane, LPG) and hydrogen with the H_2-content up to 50 volume %,
- Due to specific design of burner rig a strict control of temperature at each stage of the burner rig, flame shape and exhaust gases chemical composition is possible,
- The technological solutions applied in the burner rig allows for testing of the materials at different stages of it, i.e. inside the flame and behind it as well as in the zone of exhaust gases originated from burning of H_2-rich fuels. This in turn allows for better simulation of materials behavior used at different parts of the turbines and makes the newly developed equipment very flexible,
- Numerical modelling of temperature distribution showed significant decrease of temperature from 1674℃ in the inside of burner rig to 214℃ on steel housing.

References

Airbus (2023). *Could hydrogen fuel-cell systems be the solution for emission-free aviation?* Retrieved September 15, 2023, from https://www.airbus.com/en/newsroom/stories/2022-11-could-hydrogen-fuel-cell-systems-be-the-solution-for-emission-free

ASTM C 680–08 (2010). American Society for Testing and Materials. Standard practice for estimate of the heat gain or loss and the surface temperatures of insulated flat, cylindrical, and spherical systems by use of computer programs.

Banihabib, R., & Assadi, M. A. (2022). Hydrogen-fueled micro gas turbine unit for carbon-free heat and power generation. *Sustainability*, *14*, Article 13305. https://doi.org/10.3390/su142013305

Boeing (2010, July 14). Boeing's phantom eye ford fusion powered stratocraft. https://www.theregister.com/2010/07/13/phantom_eye_rollout/

Chen, K., Seo, D., & Canteenwalla, P. (2021). The effect of high-temperature water vapour on degradation and failure of hot section components of gas turbine engines. *Coatings*, *11*, Article 1061. https://doi.org/10.3390/coatings11091061

Chopinet, J. N., Lassoudière, F., Fiorentino, C., Alliot, P., Guedron, S., Supié, P., et al., (2011, October 3-7). Results of the Vulcain X technological demonstration. Proceedings of the 62nd International Astronautical Congress, 8, (pp. 6289-6298). International Astronautical Federation.

Churchill, S.W., & Chu, H. H. S. (1975). Correlating equations for laminar and turbulent free convection from a horizontal cylinder. *International Journal of Heat and Mass Transfer*, *18*(9), 1049-1053. https://doi.org/10.1016/0017-9310(75)90222-7

Cojocaru, M. O., Branzei, M., & Druga, L.N. (2022). Aluminide diffusion coatings on IN 718 by pack cementation. *Materials*, *15*, Article 5453. https://doi.org/10.3390/ma15155453

Cowing, K. (2012, October 16). Blue origin tests 100 k lb LOX/LH2 engine in commercial crew program. NewSpace Watch. http://archive.is/XtDg5

Decarbonization technology. Hydrogen gas turbine. (2023, September 11). https://solutions.mhi.com/power/decarbonization-technology/hydrogen-gas-turbine/

Deodeshmukh, V. P. (2013a). Long-term performance of high-temperature foil alloys in water vapor containing environment. Part I: Oxidation behavior. *Oxidation of Metals*, *79*, 567-578. https://doi.org/10.1007/s11085-012-9343-1

Deodeshmukh, V. P. (2013b). Long-term performance of high-temperature foil alloys in water vapor containing environment. Part II: Chromia vaporization behavior. *Oxidation of Metals*, *79*, 579-588. https://doi.org/10.1007/s11085-012-9344-0

England, D. M., & Virkar, A. V. (1999). Oxidation kinetics of some nickel-based superalloy foils and electronic resistance of the oxide scale formed in air part I. *Journal of The Electrochemical Society*, *146*(9), 3196–3202. https://doi.org/10.1149/1.1392454

England, D. M., & Virkar, A. V. (2001). Oxidation kinetics of some nickel-based superalloy foils in humidified hydrogen and electronic resistance of the oxide scale formed part II *Journal of The Electrochemical Society*, *148*(4), A330–A338. https://doi.org/10.1149/1.1354611

Essuman, E., Meier, G. H., Zurek, J., Hänsel, M., Norby, T., Singheiser, L., & Quadakkers, W. J. (2008). Protective and non-protective scale formation of NiCr alloys in water vapour containing high- and low-pO_2 gases. *Corrosion Science*, *50*(6), 1753–1760. https://doi.org/10.1016/j.corsci.2008.03.001

Girolamo, G. D., Brentari, A., & Serra, E. (2014). Morphology and microstructure of NiCoCrAlYRe coatings after thermal aging and growth of an Al_2O_3-Rich oxide scale. *Coatings*, *4*(4), 701-714. https://doi.org/10.3390/coatings4040701

Gnielinski, V. (1976). New equations for heat and mass transfer in the turbulent pipe and channel flow. International Chemical Engineering, 16(2), 359-368.

Golewski, P., & Sadowski, T. (2019). The Influence of TBC aging on crack propagation due to foreign object impact. *Materials*, *12*(9), Article 1488. https://doi.org/10.3390/ma12091488

Góral, M., Pytel, M., Ochal, K., Drajewicz, M., Kubaszek, T., Simka, W., & Nieuzyla, L. (2021). Microstructure of aluminide coatings modified by Pt, Pd, Zr and Hf formed in low-activity CVD process. *Coatings*, 11(4), Article 421. https://doi.org/10.3390/coatings11040421

Grilli, M. L., Valerini, D., Slobozeanu, A. E., Postolnyi, B. O., Balos, S., Rizzo, A., & Piticescu, R. R. (2021). Critical raw materials saving by protective coatings under extreme conditions: a review of last trends in alloys and coatings for aerospace engine applications. *Materials*, *14*(7), Article 1656. https://doi.org/10.3390/ma14071656

Hänsel, M., Quadakkers, W. J., Singheiser, L., & Nickel, H. (1998). Report Forschungszentrum Julich, Jul-3583, ISSN 0944-2952.

Hänsel, M., Quadakkers, W. J., & Young, D. J. (2003). Role of water vapor in chromia-scale growth at low oxygen partial pressure. *Oxidation of Metals*, *59*(3/4), 285-301. https://doi.org/10.1023/A:1023040010859

Holcomb G. R. (2008). Calculation of reactive-evaporation rates of chromia. *Oxidation of Metals*, *69*, 163-180. https://doi.org/10.1007/s11085-008-9091-4

Hydrogen fueled gas turbines. (2023, September 12). https://www.ge.com/gas-power/future-of-energy/hydrogen-fueled-gas-turb-nes?utm_campaign=h2&utm_medium=cpc&utm_source=google&utm_content=rsa&utm_term=Ge%20hydrogen%20turbines&gclid=CjwKCAiAheacBhB8EiwAItVO2z_lfkno6CHBFQBoXnpvzF9GlALjzAhJouUzlArw-J2vuC-Ncb_XsBoCKlsQAvD_BwE

Hydrogen gas turbine. The Turbotec HyTG-550. (2023, September 14). https://www.turbotec.be/hydrogen-gas-turbine/

Janakiraman, R., Meier, G. H., & Petit, F. S. (1999). The effect of water vapor on the oxidation of alloys that develop alumina scales for protection. *Metallurgical and Materials Transactions A*, 30, 2905-2913. https://doi.org/10.1007/s11661-999-0128-3

Kopec, M., Kukla, D., Yuan, X., Rejmer, W., Kowalewski, Z. L., & Senderowski, C. (2021). Aluminide thermal barrier coating for high temperature performance of MAR 247 nickel based superalloy. *Coatings*, *11*(1), 48. https://doi.org/10.3390/coatings11010048

Lele, A. (2014). GSLV-D5 success: a major “booster” to India's space program. *The Space Review*. http://www.thespacereview.com/article/2428/1

Marin, G. E., Mendeleev, D. I., & Osipov, B. M. (2021). A study on the operation of a gas turbine unit using hydrogen as fuel. Journal; of Physics: Conference Series, 1891, Article 012055. https://doi.org/10.1088/1742-6596/1891/1/012055

Maris-Sida, M. C., Meier, G. H., & Petit F. S. (2003). Some water vapor effects during the oxidation of alloys that are α-Al_2O_3 formers. *Metallurgical and Materials Transactions A*, *34*, 2609-2619. https://doi.org/10.1007/s11661-003-0020-5

Michalik, M., Hänsel, M., Zurek, J., Singheiser, L., & Quadakkers, W. J. (2005). Effect of water vapour on growth and adherence of chromia scales formed on Cr in high and low pO_2-environments at 1000 and 1050°C. *Materials and High Temperatures*, *22*(3-4) , 213-221. https://doi.org/10.1179/mht.2005.025

Moses, P. L., Rausch, V. L., Nguyen, N. T., & Hill, J. R.. (2004). NASA hypersonic flight demonstrators-overview, status, and future plans. *Acta Astronautica*, *55*(3-9), 619-630. https://doi.org/10.1016/j.actaastro.2004.05.045

Najjar, Y. S. H. (1990). Hydrogen fueled and cooled gas turbine engine. *International Journal of Hydrogen Energy*, *15*(11), 827-832. https://doi.org/10.1016/0360-3199(90)90019-U

NASA (1968) J-2 Engine fact sheet. *Saturn V News Reference*. Retrieved September 17, 2023, from http://www.nasa.gov/centers/marshall/pdf/499245mainJ2Enginefs.pdf

Nazari, M. A., Alavi, M. F., Salem, M., & El Haj Assad M. (2022). Utilization of hydrogen in gas turbines: acomprehensive review. *International Journal of Low-Carbon Technologies*, *17*, 513–519. https://doi.org/10.1093/ijlct/ctac025

Negoro, N., Ogawara, A., Onga, T., Manako, H., Kurosu, A., Yamanishi, N., Miyazaki, K., Hari, S., & Okita, K. (2007, July 8-11). Next booster engine LE-X in Japan. Proceedings of the 43rd AI-AA/ASME/SAE/ASEE Joint Propulsion Conference & Exhibit, Article AIAA 2007-5490. https://doi.org/10.2514/6.2007-5490

Nowak, W. J., Wierzba, P., Naumenko, D., Quadakkers, W. J., & Sieniawski, J. (2016). Water vapour effect on high temperature oxidation behaviour of superalloy Rene 80. Advances in Manufacturing Science and Technology, 40, 41-52. https://doi.org/10.2478/amst-2016-000

Onal, K., Maris-Sida, M. C., Meier, G. H., & Pettit, F. S. (2004). The effects of water vapor on the oxidation of nickel-base superalloys and coatings at temperatures from 700°C to 1100°C. *Superalloys*, 607-615.

Opila, E. J., Mayers, D. L., Jacobson, N. S., Nielsen, I. M. B., Johnson, D. F., Olminsky, J. K., & Allendorf, M. D. (2007). Theoretical and experimental investigation of the thermochemistry of $CrO_2(OH)_2$(g). *Journal of Physical Chemistry A*, *111*(10), 1971-1980. https://doi.org/10.1021/jp0647380

Pędrak, P., Dychtoń, K., Drajewicz, M., & Góral, M. (2021). Synthesis of $Gd_2Zr_2O_7$ coatings using the novel reactive PS-PVD Process. *Coatings*, *11*(10), Article 1208. https://doi.org/10.3390/coatings11101208

Pędrak, P., Góral, M., Dychton, K., Drajewicz, M., Wierzbinska, M., & Kubaszek, T. (2022). The influence of reactive PS-PVD process parameters on the microstructure and thermal properties of $Yb_2Zr_2O_7$ thermal barrier coating. *Materials*, *15*(4), Article 1594. https://doi.org/10.3390/ma15041594

Pujilaksono, B., Jonsson, T., Halvarsson, M., Panas, I., Svensson, J. E., & Johansson, L. G. (2008). Paralinear oxidation of chromium in O_2 + H_2O environment at 600-700°C. *Oxidation of Metals*, *70*, 163-188. https://doi.org/10.1007/s11085-008-9114-1

Pyo, M.-J., Moon, S.-W., & Kim, T.-S. (2021). A comparative feasibility study of the use of hydrogen produced from surplus wind power for a gas turbine combined cycle power plant. *Energies*, *14*(24), Article 8342. https://doi.org/10.3390/en14248342

Qiu, S.-Y., Wu, C.-W., Huang, C.-G., Ma, Y., & Guo, H.-B. (2021). Microstructure dependence of effective thermal conductivity of EB-PVD TBCs. *Materials*, *14*(8), 1838. https://doi.org/10.3390/ma14081838

Quaddakers, W. J., Norton, J. F., Canetoli, S., Schuster, K., & Gil, A. (1996). In S. B. Newcomb, J. A. Little, (Eds.); 3rd International Conference on Microscopy of Oxidation (pp. 609-619). The Institute of Materials.

Rachuk, V., Goncharov, N., Martinyenko, Y., & Fanciullo, T. (1996, July 1-3). Evolution of the RD-0120 for future launch systems. Proceedings of the 32nd Joint Propulsion Conference and Exhibit Article 96-3004. https://doi.org/10.2514/6.1996-3004

Renouard-Vallet, G., Kallo. J., Saballus, M., Schmithals, G., Schirmer, J., & Friedrich, K.A. (2011). Fuel cells for aircraft applications. *ECS Transactions*, *30*, 271-280. https://doi.org/10.1149/1.3562482

Report 2555-M-1-F. (1967). *Development of a 1,500,000-lb-thrust (nominal vacuum) liquid hydrogen/liquid oxygen engine*. (August 1967). Retrieved September 16, 2023, from http://alternatewars.com/BBOW/Space_Engines/1967_M-1_Final_Report.pdf

Rich, B.R. (1973, May 15-16). Lockheed CL-400 liquid hydrogen fueled Mach 2.5 reconnaissance vehicle. Symposium on hydrogen fueled aircraft.

Schütze, M., & Quadakkers, W. J. (2017). Future directions in the field of high-temperature corrosion research. *Oxidation of Metals*, *87*, 681–704. https://doi.org/10.1007/s11085-017-9719-3

Smialek, J. L. (2010). Moisture-induced alumina scale spallation: The hydrogen factor. Report NASA/TM-2010-216260 (pp. (1-31).Retrieved September 4, 2023, from https://ntrs.nasa.gov/api/citations/20100021167/downloads/20100021167.pdf

Southern Co. Gas-fired demonstration validates 20% hydrogen fuel blend. (2023, September 13). https://www.powermag.com/southern-co-gas-fired-demonstration-validates-20-hydrogen-fuel-blend/

Stanislowski, M., Froitzheim, J., Niewolak, L., Quadakkers, W. J., Hilpert, K., Markus, T., & Singheiser L. (2007). Reduction of chromium vaporisation from SOFC interconnectors by highly effective coatings. *Journal of Power Sources*, *164*(2), 578-589. https://doi.org/10.1016/j.jpowsour.2006.08.013

Stefan, E., Talic, B., Larring, Y., Gruber, A., & Peters, T. A. (2022). Materials challenges in hydrogen-fuelled gas turbines, International Materials Reviews, 67(5), 461-486. https://doi.org/10.1080/09506608.2021.1981706

Suzuki, M., Shahien, M., Shinoda, K., & Akedo, J. (2022) The current status of environmental barrier coatings and future direction of thermal spray process. *Materials Transactions*, 63(8), 1101-1111. https://doi.org/10.2320/matertrans.MT-T2021003

Tan, Y.H. (2013). Research on large thrust liquid rocket engine. *Yuhang Xuebao/Journal of Astronautics*, *34*(10), 1303-1308. http://dx.doi.org/10.3873/j.issn.1000-1328.2013.10.002

Tupolev, A.A., (1994). Utilization of liquid hydrogen or liquid natural gas as an aviation fuel. In R. E. Billings, E. Dayton (Eds.). *Conference proceedings, Project Energy* (p. 104). International Academy of Sciences.

Vassen, R., Bakan, E., Gatzen, C., Kim, S., Mack, D.E., & Guillon, O. (2019). Environmental barrier coatings made by different thermal spray technologies. *Coatings*, *9*(12), Article 784. https://doi.org/10.3390/coatings9120784

Wang, C., Liu, M., Feng, J., Zhang, X., Deng, C., Zhou, K., Zeng, D., Guo, S., Zhao, R., & Li, S. (2020). Water vapor corrosion behavior of Yb_2SiO_5 environmental barrier coatings prepared by plasma spray-physical vapor deposition. *Coatings*, *10*(4), 392. https://doi.org/10.3390/coatings10040392

Westenberger, A. (2002). Liquid hydrogen fuelled aircraft-system analysis. Final technical report 2002.

Westenberger, A. (2003). Liquid hydrogen fuelled aircraft-system analysis. Final technical report (publishable version). Cryoplane project, 2003.

Wilhelm, W. F. (1972). Space shuttle orbiter main engine design. *Society of Automotive Engineers Transactions*, *81*, Article 72 0807.

Winter, C. J. (1990). Hydrogen in high speed air transportation. *International Journal of Hydrogen Energy*, *15*(8), 579-595. https://doi.org/10.1016/0360-3199(80)90006-3

Zakeri, A., Bahmani, E., & Ramazani, A. (2022). A review on the enhancement of mechanical and tribological properties of MCrAlY coatings reinforced by dispersed micro and nanoparticles. *Energies*, *15*(5), 1914. https://doi.org/10.3390/en15051914

Zero emission hydrogen turbine center. (2023, September 12). https://www.siemens-energy.com/global/en/priorities/future-technologies/hydrogen/zehtc.html

Żurek, J., Young, D. J., Essuman, E., Hänsel, M., Penkalla, H. J., Niewolak, L., & Quadakkers, W. J. (2008). Growth and adherence of chromia based surface scales on Ni-base alloys in high- and low-pO_2 gases. *Materials Science and Engineering A*, *477*(1-2), 259-270. https://doi.org/10.1016/j.msea.2007.05.035

Charakterystyka badawczego stanowiska palnikowego zasilanego paliwem wodorowym dedykowanego do badań materiałów

Streszczenie

Głównym celem niniejszego artykułu jest przedstawienie stanowiska palnikowego nowo opracowanego na Politechnice Rzeszowskiej. Palnik przeznaczony jest do pracy na paliwach bogatych w wodór. Palnik może pracować z paliwami o zawartości wodoru do 50% obj. Przedstawiono szczegółowy opis budowy stanowiska palnika. Zaprezentowano także model matematyczny przewidujący rozkład temperatury w komorze spalania. Uzyskane wyniki wykazały dobrą izolację konstrukcji palnika, co doprowadziło do powstania gradientu temperatury od 1674°C w korpusie palnika do 214°C na obudowie stalowej.

Słowa kluczowe: paliwo wodorowe; stanowisko badawcze; korozja gazowa, para wodna, materiały żaroodporne.